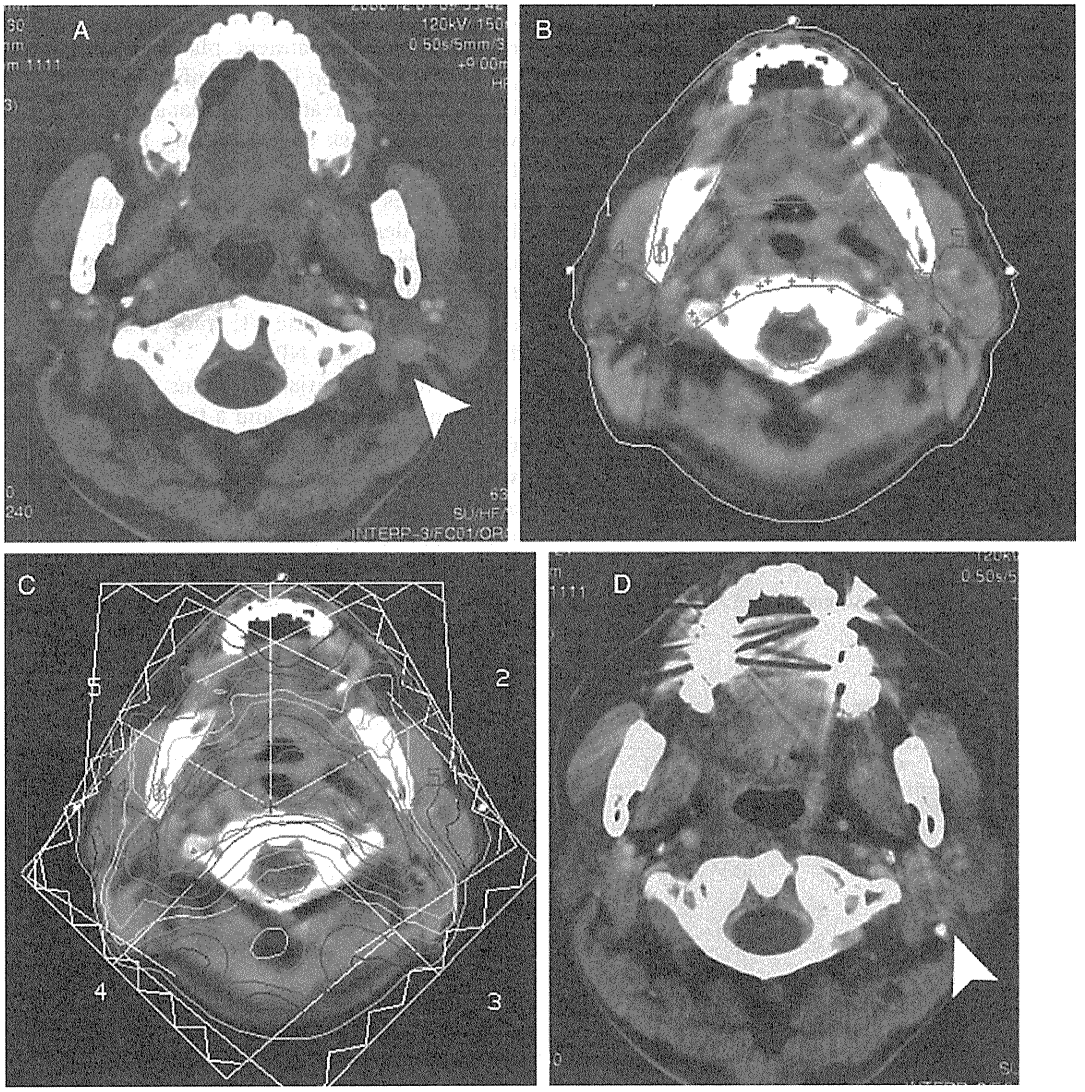

Figure 4. A 63-year-old man with NPC (T4N2M0). This patient was treated with 66 Gy/35 fractions and concurrent cisplatin of 370 mg in three courses. (A) Computed tomography before IMRT showing lt periparotid lymph node of 7 mm in diameter. (B) Red line indicates PTV, which misses the periparotid lymph node. (C) Isodose curves. The lt periparotid lymph node was located at the dose gradient region between PTV and the lt parotid grand. (D) Fourteen months after the start of IMRT, computed tomography showed recurrence of the lt periparotid lymph node. Re-irradiation was done for the recurrent lymph node.

Table 3 shows the acute toxicities associated with IMRT with or without concurrent chemotherapy. Hematological toxicities were mild, and no Grade 4 hematological toxicity was noted. Two patients showed Grade 4 mucositis. One patient with Grade 4 mucositis refused CRT after 60 Gy with two doses of concurrent cisplatin, and this patient required interruption of RT for 22 days. Sepsis with high fever of Grade 4 toxicity was noted immediately after the first chemotherapy in one patient. RT was interrupted for 10 days for this patient. Except for the two patients, no treatment interruption due to acute toxicities was necessary, and the median overall treatment time was 51 days (Table 2).

Late toxicities associated with IMRT with or without concurrent chemotherapy are shown in Table 4. Hearing difficulty, tinnitus and otitis were common late toxicities. However, most patients with auditory toxicities had the same symptom at presentation. Although several patients complained of dysphagia after treatment, no patient needed percutaneous endoscopic gastrostomy. One patient died of suffocation by food 3 months after the end of IMRT without evidence of disease. Except for the patient with early death, xerostomia scores at 1–2 years were: Grade 0, 11; Grade 1, 17; Grade 2, 5; Grade 3, 1. The patent with Grade 3 xerostomia was treated by conventional RT followed by boost IMRT.

Table 3. Acute toxicities (CTCAE, version 3.0)

Toxicities	G2	G3	G4
WBC	16	10	0
Hb	11	0	0
Plt	0	1	0
Mucositis	16	13	2
Dysphagia	19	14	0
Dermatitis	8	2	0
Nausea	22	9	0
Vomiting	16	1	0
Infection	0	1	1
Fever	3	0	1
Fatigue	0	1	0
Creatinine	1	0	0
Liver	2	0	0

CTCAE, Common Toxicity Criteria for Adverse Events; WBC, white blood cells; Hb, hemoglobin; Plt, platelets.

Table 4. Late toxicities (CTCAE, version 3.0)

Toxicities	G1	G2	G3	G4	G5
Hearing	0	5	1	1	0
Tinnitus	0	6	0	0	0
Otitis, middle ear	1	5	0	0	0
Xerostomia at 12–24 months	17	5	1	0	0
Dysphagia	4	3	0	0	1?
Pharyngeal wall	5	0	1	0	0
Larynx	11	0	0	0	0
Hypothyroidism	0	2	0	0	0
Skin	1	0	0	0	0
Creatinine	1	0	0	0	0

DISCUSSION

Clinical results of our adaptive RT scheme of a two-step IMRT method for NPC were analyzed in the present study, and excellent overall survival and loco-regional control rates were obtained when concurrent chemotherapy was combined with IMRT. When introducing IMRT for head and neck cancers at our hospital, we chose a most conservative method, although it is a time-consuming strategy. Inverse planning for IMRT was performed twice. This two-step IMRT method obviously took a longer time for the treatment planning and QA than a single-step simultaneous integrated boost (SIB) method which gives several dose levels for CTVs and GTV simultaneously (8,10,11,14). It took 5 working days at our institution for the inverse planning and its verification, and the IMRT plan was started 7–10 days after CT simulation. Because CT-2 for boost IMRT plan was performed at an RT dose of 36–40 Gy, no treatment interruption due to treatment planning was inserted for all patients. A two-step IMRT method has an advantage, in that it can adapt the treatment to changes in body contour, target volumes and risk organs during IMRT. As patients with locally advanced NPC frequently appeared with large neck lymph nodes swelling and as both primary tumors and neck lymph nodes regress rapidly by RT, a two-step IMRT method is especially desirable for locally advanced NPC. In the only other report of a two-step IMRT method, Lee et al. (13) described a Phase I/II study of a two-step SIB method for 20 patients with NPC.

No direct comparison in terms of clinical or DVH results between a single-step and a two-step IMRT was shown in the present study, because all patients with NPC were treated with a two-step IMRT method at our institution. We do not argue a two-step IMRT method is a new standard method of IMRT. A two-step method has been used in the conventional RT for head and neck cancer. Thus, a two-step IMRT method is a conventional and conservative method of IMRT compared with a single-step SIB IMRT method with larger fraction sizes for GTV. For early-stage NPC with T1,2N0M0 disease, effects of tumor regression during IMRT may be small, and a single-step method may be applicable. In fact, a single-step SIB IMRT method is applied for early oropharyngeal cancer (T1,2N0,1M0) at our institution. However, even for patients with early NPC, body weight and contour can be changed when concurrent CRT is used. Therefore, we consider that a two-step IMRT method is one of the safe methods of IMRT for patients with NPC treated by concurrent CRT.

In our early cases, PTV marginal recurrence was noted in three patients (9%). There may be several reasons for the early marginal recurrence. In our first TPS (Cadplan Helios), the function of adding a margin to CTV or GTV was lacking, i.e. PTV was contoured directly at that time (Figs 3 and 4). In two of the three patients with marginal recurrences, pre-treatment MRI or CT scan of the patients could depict the involved nodes or the extension of the primary tumor. Precise contouring of CTV and PTV based on various imaging modalities including MRI and FDG-PET is most important for the success of IMRT. TPS was changed to the second generation type (Eclipse) in 2004 and PTV margins of 3–5 mm were added to CTV (28). In addition, an integrated PET-CT simulation was started in 2006 (22,23). PET-CT simulation was especially effective to depict GTV invading the skull base. Along with improvements in equipment and knowledge of contouring, PTV marginal recurrence has never occurred since 2003.

Only six patients (18%) complained of Grade 2 or 3 xerostomia 1–2 years after IMRT. Thus, a two-step IMRT is also effective for preventing xerostomia. One notable late toxicity is dysphagia. Recently, several investigators have noted the importance of the RT dose to the pharyngeal constructors (30–32). Seven patients complained of Grade 1 or 2 dysphagia, and one patient died of suffocation by food

3 months after the end of IMRT without evidence of the disease. As this patient had complained of dysphagia, this accident may have been a treatment-related death (Grade 5 toxicity).

In conclusion, excellent overall survival and local-PFS rates were obtained by a two-step IMRT method with concurrent chemotherapy for NPC. This two-step IMRT method as an adaptive RT scheme could correspond to changes in body contour, target volumes and risk organs during IMRT. A prospective multi-institutional clinical trial of a two-step IMRT method for NPC is warranted.

Funding

This study was partially supported by a Grant-in-Aid for Scientific Research (17591300) from the Ministry of Education, Culture, Sports, Science and Technology, Japan, and a Grant-in-Aid for Cancer Research (20S-5) from the Ministry of Health, Labor and Welfare, Japan.

Conflict of interest statement

None declared.

References

1. Baujat B, Audry H, Bourhis J, Chan AT, Onat H, Chua DT, et al. Chemotherapy in locally advanced nasopharyngeal carcinoma: an individual patient data meta-analysis of eight randomized trials and 1753 patients. *Int J Radiat Oncol Biol Phys* 2006;64:47–56.
2. Al-Sarraf M, LeBlanc M, Giri PG, Fu KK, Cooper J, Vuong T, et al. Chemoradiotherapy versus radiotherapy in patients with advanced nasopharyngeal cancer: phase III randomized Intergroup Study 0099. *J Clin Oncol* 1998;16:1310–7.
3. Chen Y, Liu MZ, Liang SB, Zong JF, Mao YP, Tang LL, et al. Preliminary results of a prospective randomized trial comparing concurrent chemoradiotherapy plus adjuvant chemotherapy with radiotherapy alone in patients with locoregionally advanced nasopharyngeal carcinoma in endemic regions of China. *Int J Radiat Oncol Biol Phys* 2008;71:1356–64.
4. Wee J, Tan EH, Tai BC, Wong HB, Leong SS, Tan T, et al. Randomized trial of radiotherapy versus concurrent chemoradiotherapy followed by adjuvant chemotherapy in patients with American Joint Committee on Cancer/International Union against cancer stage III and IV nasopharyngeal cancer of the endemic variety. *J Clin Oncol* 2005;23:6730–8.
5. Lin JC, Jan JS, Hsu CY, Liang WM, Jiang RS, Wang WY. Phase III study of concurrent chemoradiotherapy versus radiotherapy alone for advanced nasopharyngeal carcinoma: positive effect on overall and progression-free survival. *J Clin Oncol* 2003;21:631–7.
6. Pow EH, Kwong DL, McMillan AS, Wong MC, Sham JS, Leung LH, et al. Xerostomia and quality of life after intensity-modulated radiotherapy vs. conventional radiotherapy for early-stage nasopharyngeal carcinoma: initial report on a randomized controlled clinical trial. *Int J Radiat Oncol Biol Phys* 2006;66:981–91.
7. Kam MK, Leung SF, Zee B, Chau RM, Suen JJ, Mo F, et al. Prospective randomized study of intensity-modulated radiotherapy on salivary gland function in early-stage nasopharyngeal carcinoma patients. *J Clin Oncol* 2007;25:4873–9.
8. Lee N, Xia P, Quivey JM, Sultanem K, Poon I, Akazawa C, et al. Intensity-modulated radiotherapy in the treatment of nasopharyngeal carcinoma: an update of the UCSF experience. *Int J Radiat Oncol Biol Phys* 2002;53:12–22.
9. Fang FM, Chien CY, Tsai WL, Chen HC, Hsu HC, Lui CC, et al. Quality of life and survival outcome for patients with nasopharyngeal carcinoma receiving three-dimensional conformal radiotherapy vs. intensity-modulated radiotherapy—a longitudinal study. *Int J Radiat Oncol Biol Phys* 2008;72:356–64.
10. Wolden SL, Chen WC, Pfister DG, Kraus DH, Berry SL, Zelefsky MJ. Intensity-modulated radiation therapy (IMRT) for nasopharynx cancer: update of the Memorial Sloan-Kettering experience. *Int J Radiat Oncol Biol Phys* 2006;64:57–62.
11. Kwong DL, Sham JS, Leung LH, Cheng AC, Ng WM, Kwong PW, et al. Preliminary results of radiation dose escalation for locally advanced nasopharyngeal carcinoma. *Int J Radiat Oncol Biol Phys* 2006;64:374–81.
12. Lee AW, Lau KY, Hung WM, Ng WT, Lee MC, Choi CW, et al. Potential improvement of tumor control probability by induction chemotherapy for advanced nasopharyngeal carcinoma. *Radiother Oncol* 2008;87:204–10.
13. Lee SW, Back GM, Yi BY, Choi EK, Ahn SD, Shin SS, et al. Preliminary results of a phase I/II study of simultaneous modulated accelerated radiotherapy for nondisseminated nasopharyngeal carcinoma. *Int J Radiat Oncol Biol Phys* 2006;65:152–60.
14. Kam MK, Teo PM, Chau RM, Cheung KY, Choi PH, Kwan WH, et al. Treatment of nasopharyngeal carcinoma with intensity-modulated radiotherapy: the Hong Kong experience. *Int J Radiat Oncol Biol Phys* 2004;60:1440–50.
15. Mendenhall WM, Mancuso AA. Radiotherapy for head and neck cancer; is the 'next level' down? *Int J Radiat Oncol Biol Phys* 2009;73:645–6.
16. Mendenhall WM, Amdur RJ, Palta JR. Intensity-modulated radiotherapy in the standard management of head and neck cancer: promises and pitfalls. *J Clin Oncol* 2006;24:2618–23.
17. Harari PM. Beware the swing and a miss: baseball precautions for conformal radiotherapy. *Int J Radiat Oncol Biol Phys* 2008;70:657–9.
18. Barker JL Jr, Garden AS, Ang KK, O'Daniel JC, Wang H, Court LE, et al. Quantification of volumetric and geometric changes occurring during fractionated radiotherapy for head-and-neck cancer using an integrated CT/linear accelerator system. *Int J Radiat Oncol Biol Phys* 2004;59:960–70.
19. Nishimura Y, Nakamatsu K, Shibata T, Kanamori S, Koike R, Okumura M, et al. Importance of the initial volume of parotid glands in xerostomia for patients with head and neck cancers treated with IMRT. *Jpn J Clin Oncol* 2005;35:375–79.
20. Cannon DM, Lee NY. Recurrence in region of spared parotid gland after definitive intensity-modulated radiotherapy for head and neck cancer. *Int J Radiat Oncol Biol Phys* 2008;70:660–5.
21. Schoenfeld GO, Amdur RJ, Morris CG, Li JG, Hinerman RW, Mendenhall WM. Patterns of failure and toxicity after intensity-modulated radiotherapy for head and neck cancer. *Int J Radiat Oncol Biol Phys* 2008;71:377–85.
22. Okubo M, Nishimura Y, Nakamatsu K, Okumura M, Shibata T, Kanamori S, et al. Static and moving phantom studies for radiation treatment planning in a positron emission tomography and computed tomography (PET/CT) system. *Ann Nucl Med* 2008;22:579–86.
23. Okubo M, Nishimura Y, Nakamatsu K, Okumura M, Shibata T, Kanamori S, et al. Radiation treatment planning using positron emission and computed tomography (PET/CT) for lung and pharyngeal cancers: a multiple thresholds method for FDG activity. *Int J Radiat Oncol Biol Phys*; in press.
24. Isobe K, Kawakami H, Uno T, Yasuda S, Aruga T, Ueno N, et al. Concurrent chemoradiotherapy for locoregionally advanced nasopharyngeal carcinoma: is Intergroup Study 0099 feasible in Japanese patients? *Jpn J Clin Oncol* 2003;33:497–500.
25. Tang L, Li L, Mao Y, Liu L, Liang S, Chen Y, et al. Retropharyngeal lymph node metastasis in nasopharyngeal carcinoma detected by magnetic resonance imaging. *Cancer* 2008;113:347–54.
26. Zheng XK, Chen LH, Wang QS, Wu HB, Wang HM, Chen YQ, et al. Influence of FDG-PET on computed tomography-based radiotherapy planning for locally recurrent nasopharyngeal carcinoma. *Int J Radiat Oncol Biol Phys* 2007;69:1381–8.
27. Eisbruch A, Foote RL, O'Sullivan B, Beitler JJ, Vikram B. Intensity-modulated radiation therapy for head and neck cancer: emphasis on the selection and delineation of the targets. *Semin Radiat Oncol* 2002;12:238–49.

28. Suzuki M, Nishimura Y, Nakamatsu K, Okumura M, Hashiba H, Koike R, et al. Analysis of interfractional set-up errors and intrafractional organ motions during IMRT for head and neck tumors to define an appropriate planning target volume (PTV)- and planning organs at risk volume (PRV)-margins. *Radiother Oncol* 2006;78:283–90.
29. Suzuki M, Nakamatsu K, Kanamori S, Okumura M, Uchiyama T, Akai F, et al. Feasibility study of the simultaneous integrated boost (SIB) method for malignant gliomas using intensity modulated radiotherapy (IMRT). *Jpn J Clin Oncol* 2003;33:271–7.
30. Teguh DN, Levendag PC, Noever I, van Rooij P, Voet P, van der Est H, et al. Treatment techniques and site considerations regarding dysphagia-related quality of life in cancer of the oropharynx and nasopharynx. *Int J Radiat Oncol Biol Phys* 2008;72:1119–27.
31. Eisbruch A, Schwartz M, Rasch C, Vineberg K, Damen E, Van As CJ, et al. Dysphagia and aspiration after chemoradiotherapy for head-and-neck cancer: which anatomic structures are affected and can they be spared by IMRT? *Int J Radiat Oncol Biol Phys* 2004;60:1425–39.
32. Caglar HB, Tishler RB, Othus M, Burke E, Li Y, Goguen L, et al. Dose to larynx predicts for swallowing complications after intensity-modulated radiotherapy. *Int J Radiat Oncol Biol Phys* 2008;72:1110–8.

IOP PUBLISHING PHYSICS IN MEDICINE AND BIOLOGY

Phys. Med. Biol. **55** (2010) 3101–3113 doi:10.1088/0031-9155/55/11/008

The effect of gantry and collimator angles on leaf limited velocity and position in dynamic multileaf collimator intensity-modulated radiation therapy

M Okumura[1,2], Y Obata[3], K Shimomura[2], M Tamura[4] and Y Nishimura[4]

[1] Program in Radiological and Medical Laboratory Sciences, Nagoya University Graduate School of Medicine, Nagoya, Japan
[2] Department of Radiological Service, Kinki University Hospital, Osaka, Japan
[3] Department of Radiological Technology, Nagoya University School of Health Sciences, Nagoya, Japan
[4] Department of Radiation Oncology, Kinki University, Osaka, Japan

E-mail: m_okumura@w2.dion.ne.jp

Received 18 February 2010, in final form 14 April 2010
Published 12 May 2010
Online at stacks.iop.org/PMB/55/3101

Abstract

The purpose of the study is to evaluate the limiting velocity (LV) of a multileaf collimator and the leaf position in various collimator and gantry angles. Both leading leaves and trailing leaves began to move with a constant acceleration from 0 to 4 cm s^{-1}. When the beam hold occurred, the leaf velocity was defined as the leaf LV. Dynamic irradiation was performed at eight gantry angles of every 45° with three different collimator angles. The analysis of the LV and the leaf position was performed with a log file from a leaf motion controller. The mean LVs for Varian Clinac 21EX (21EX) ranged from 2.51 to 3.10 cm s^{-1}. The mean LVs for Clinac 600C ranged from 2.91 to 3.12 cm s^{-1}. When only central 5 mm leaves of 21EX moved, LVs were significantly higher than those when all 60 pairs of leaf moved, while the leaf position inconsistencies of the two accelerators were within 1 mm at the leaf velocities from 0.5 to 2.0 cm s^{-1}. It was recognized that the LV was affected by gravity. This measurement method can be utilized as routine quality assurance for a dynamic multileaf collimator (DMLC) is and easily reproducible.

1. Introduction

Intensity-modulated radiation therapy (IMRT) has been widely used and clinical advantages have been demonstrated for some anatomic sites (Mell *et al* 2005, Lee *et al* 2002, Mundt *et al* 2002, Chao *et al* 2001, Zelefsky *et al* 2002). Nearly all IMRT is delivered using a multileaf collimator (MLC), which can be employed in two basic modes, segmental IMRT (also known

0031-9155/10/113101+13$30.00

as step and shoot), in which the leaves do not move while the beam is on, and dynamic MLC (DMLC) IMRT, in which the leaves move during irradiation. In DMLC-IMRT, leaf velocity, leaf position accuracy, leaf gap width and dose rate stability all affect the dose distribution and radiation output. Even an error of ± 0.2 mm in the gap width causes a significant dose error of approximately 3% (Ezzell *et al* 2003, LoSasso *et al* 1998, Zhu *et al* 2002, Chui *et al* 1996). Compared with segmental MLC-IMRT, in DMLC IMRT the tolerance level and action level of the MLC position and gap width require a twofold constriction in accuracy (Palta *et al* 2003). Before the clinical delivery of an optimized and approved IMRT plan, it is recommended that the dosimetry of the IMRT plan should be verified. The dose distribution and radiation output of each beam are generally measured at a gantry angle of 0° using an ionization chamber dosimeter, films, electronic portal-imaging device (EPID) and/or a 2D array detector (LoSasso *et al* 2001, Jursinic and Nelms 2003, Greer and Popescu 2003, Buonamici *et al* 2007).

In the current Varian architecture (Varian Medical Systems, Palo Alto, CA), a leaf motion controller (LMC) controls the position and motion of each leaf. During a DMLC delivery, the LMC monitors the actual leaf position against the expected position every 50 ms, and corrects any discrepancy by pausing the beam, issuing a 'beam hold' condition. This beam hold depends on the physical maximum velocity and the travel distance during each segment of the DMLC delivery, and the selected dose rate in the treatment planning system (TPS). For a given plan, since the leaves are always set to move toward the same direction relative to the isocenter, the leaf movement for the gantry angle of 90° is opposite to that required for 270°. The load on the leaf motor due to gravity of the leaf can be changed because of differences in the leaf speed (Wijesooriya *et al* 2005). Recently, intensity-modulated arc therapy (IMAT) or volumetric-modulated arc therapy (VMAT), which also uses dynamic beam irradiation, has been commercialized (Yu 1995, Otto 2008). However, the gantry or collimator angular dependence on the actual DMLC delivery is not corrected by the TPS.

In the present study, a DMLC file in which the leaf velocity is constantly accelerated was created using the Shaper software (Varian Medical Systems, Palo Alto, CA), and the dynamic irradiation was delivered at various collimator and gantry angles. Special attention was paid to assess the angular dependence of the physical characteristics of the MLC using a log file (Varian Medical Systems, Palo Alto, CA).

2. Materials and methods

2.1. Linear accelerators and the DMLC file

A Varian Clinac 21EX accelerator (CLINAC-21EX) and Clinac 600C accelerator (CLINAC-600C) (Varian Medical Systems, Palo Alto, CA) were used in the present study. The x-ray energy for the CLINAC-21EX was 6 MV and that for CLINAC-600C was 4 MV. Our CLINAC-21EX is equipped with a Millennium 120 leaf MLC (40 central pairs of 5 mm width leaves and 20 peripheral pairs of 10 mm width leaves) and CLINAC-600C with Millennium 80 leaf MLCs (40 pairs of 10 mm leaves). Both of the MLC software versions were 6.8. When the carriage supporting the MLC was fixed, the maximum range of the leaf movement was 15.0 cm at the isocenter.

In the DMLC file plan made for this study, the range of movement for the leading leaf bank was from -6.20 to 6.25 cm and that for the trailing leaf bank was from -6.25 to 6.20 cm. The DMLC file was divided into 166 control points. The gap width for all leaves was 0.05 cm at the beginning, and leading leaves started to move when the radiation beam was turned on. When the leaves' gap width became 5 mm, both leading leaves and trailing leaves began to move parallel with a constant acceleration from 0 to 4 cm s^{-1} at the isocenter. For

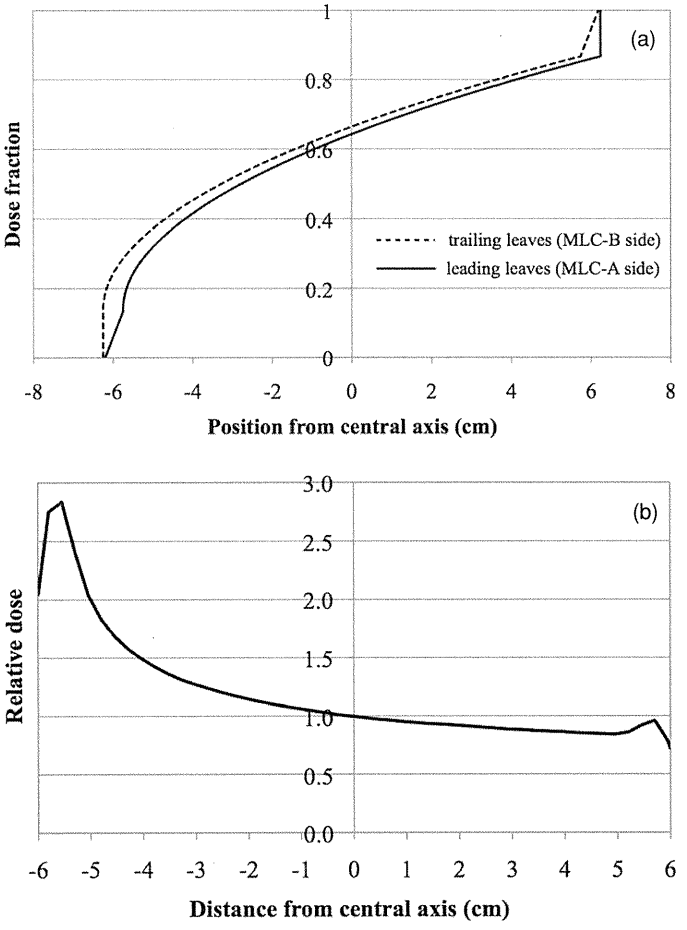

Figure 1. (a) The leaf positions of each control point of the DMLC files (the leaf positions show the distance from the central axis). (b) Calculated intensity profile for 6 MV x-ray along the leaf motion direction at the depth of the peak.

the CLINAC-21EX, two DMLC files were made: one in which all 60 pairs of 5 and 10 mm leaves were moved, and one in which only the 40 central pairs of 5 mm leaves were moved. For CLINAC-600C, one DMLC file was made for the movement of all 40 pairs of 10 mm leaves. The dynamic leaf position tolerance was set at 2 mm. This means that radiation beam hold occurred when the difference between the expected leaf position and the actual position exceeded 2 mm.

Figure 1 shows the leaf positions of each control point of the DMLC files and calculated intensity profile for 6 MV x-ray along the leaf motion direction at the depth of the peak. Figure 2 shows the planned velocity of the leading leaves according to the elapsed time. When the leaf velocity was accelerated constantly from 0 to 4 cm s^{-1} for the distance of 12 cm at the isocenter, in the case of a constant dose rate, the monitor unit (MU) was determined directly. In other words, the rate of acceleration can be changed by varying the value of the dose rate or MU. In this study, the calculated MU for CLINAC-21EX was 40 at a dose rate of 300 MU min^{-1}, and that for CLINAC-600C was 34 at a dose rate of 250 MU min^{-1}. The dynamic irradiation was performed every 45° between 0° and 315° of gantry angle with

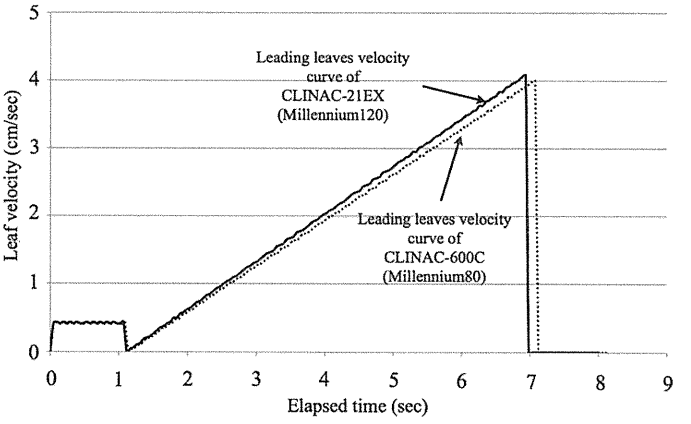

Figure 2. The planned velocity of the leading leaves according to the elapsed time.

collimator angles of 0°, 45° and 315°. For each gantry and collimator angle, the dynamic irradiation was given 15 times and their log files were obtained.

2.2. Analysis of log files

Log files recorded in the LMC were used to evaluate MLC performance. The accuracy of the log files for the linear accelerators was previously verified by film, diode array and electronic portal imaging devices (Stell *et al* 2004, Li *et al* 2003, Zygmanski *et al* 2003, Zeidan *et al* 2004). Log files consist of a text format which includes the leaf positions of the MLC, the beam state and other information, and they have been used for the physical evaluation and validation of MLC performance (Litzenberg *et al* 2002b). During the dynamic irradiation, expected and actual positions of leaves were recorded every 50 ms by signals from the MLC motor (primary feedback). The 50 ms in the log file is a delay time between the accelerator and LMC response to a given condition. Therefore, the expected and actual positions of the leaves from the log files created from each delivery show that actual leaf positions always lag their expected positions for at least one check cycle (Litzenberg *et al* 2002a).

For this study, we wrote an in-house program which extracted the data on the beam state, as well as the expected and actual positions of the leaves every 50 ms, from the log files. To calculate positions and velocity of leaves at the isocenter level, leaves' position data in log files were multiplied by a geometric magnification factor of 1.96 based on the relationship of the radiation source-to-MLC-isocenter distance (the radiation source to the MLC distance was 51.0 cm and the MLC to isocenter distance was 49.0 cm).

Figure 3 shows an example of the relationship between the planned leaf velocity of the DMLC file, the actual leaf velocity and the actual beam state (beam hold). When the leaf velocity increased and the position error between the expected and actual positions is beyond the dynamic leaf tolerance, beam hold occurs. In the present study, when beam hold occurred, the leaf velocity was defined as the leaf limiting velocity (LV). Leaf LVs, the difference in the gap width and leaf position inconsistencies were measured for eight gantry angles of every 45° with three different collimator angles. The leaf LVs of two accelerators were calculated from the time of beam hold. The LV of the leaf was measured 15 times for each gantry angle. The difference in the leaf gap widths and leaf position inconsistencies were calculated at leaf velocities of 0.5 cm s^{-1}, 1.0 cm s^{-1}, 1.5 cm s^{-1}, 2.0 cm s^{-1} and 2.5 cm s^{-1} in log files.

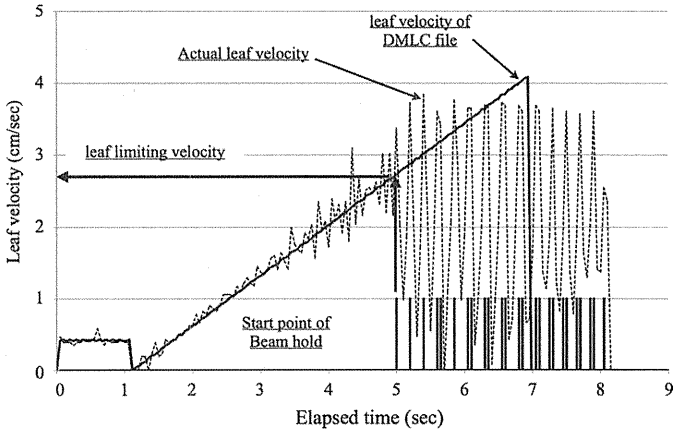

Figure 3. An example of the relationship between the planned leading leaf velocity, the actual leading leaf velocity and the actual beam state (beam hold).

3. Results

The mean leaf LVs at each gantry angle with three collimator angles of 0°, 45° and 315° were measured. Figure 4 shows the mean leaf LVs for CLINAC-21EX when all leaves were moved. Figure 5 shows the mean leaf LVs for CLINAC-600C. The mean leaf -LVs for CLINAC-21EX ranged from 2.51 to 3.10 cm s^{-1}, and the minimum LV was observed at a gantry angle of 270° with a collimator angle of 0°. The mean leaf -LVs of CLINAC-600C ranged from 2.91 to 3.12 cm s^{-1}, and the minimum LV was noted at a gantry angle of 315° with a collimator angle of 0°. The gantry angle and collimator angle dependence of the LV were not as apparent for CLINAC-600C as for CLINAC-21EX. For both accelerators, the minimum LVs were noted when the leaves moved upward against gravity. The gantry angle dependence of the leaf LV was also affected by the collimator angles, and a decline in the LV was most significant at collimator angles of 45° and 315° compared with a collimator angle of 0°. LVs at the gantry angles of 45–135° ($n = 45$) and 225–315° ($n = 45$) were compared for both accelerators. For CLINAC-21EX with all three collimator angles, the mean LV at angles of 225–315° was significantly lower than that at angles of 45–135° (Student's t-test; $p < 0.001$). A significant difference for CLINAC-600C was also noted ($p < 0.01$).

Figure 6 shows results of LVs for CLINAC-21EX when all 60 pairs of leaves or only 40 central pairs of 5 mm leaves moved. When only central 5 mm leaves moved, LVs were significantly higher than those when all 60 pairs of leaves moved. In addition, the dependence of LVs on the gantry and collimator angle was decreased when only 5 mm leaves moved, although a significant difference between 45–135° of gantry angle and 225–315° of gantry angle was still noted ($p < 0.01$). Table 1 is a summary of the LVs of leaves in three collimator angles for two accelerators obtained from figures 4, 5 and 6.

Figure 7 shows the difference in the MLC position between the expected and actual position for each leaf pair for CLINAC-21EX when beam hold occurred. The measured data in figure 7 show one example of 15 measurements. For most instances in CLINAC-21EX, the beam hold occurred due to a leaf position error in the peripheral leaves, while leaf position inconsistency was predominantly noted for the peripheral 10 mm leaves compared with the central 5 mm leaves. All results measured with CLINAC-21EX showed the same trend.

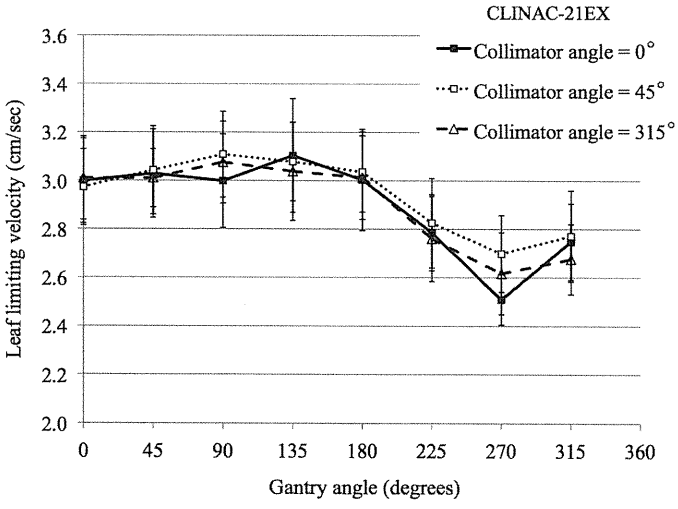

Figure 4. The mean leaf LVs at each gantry angle with three collimator angles of 0°, 45° and 315° for CLINAC-21EX when all leaves were moved. Error bars shown correspond to one standard deviation.

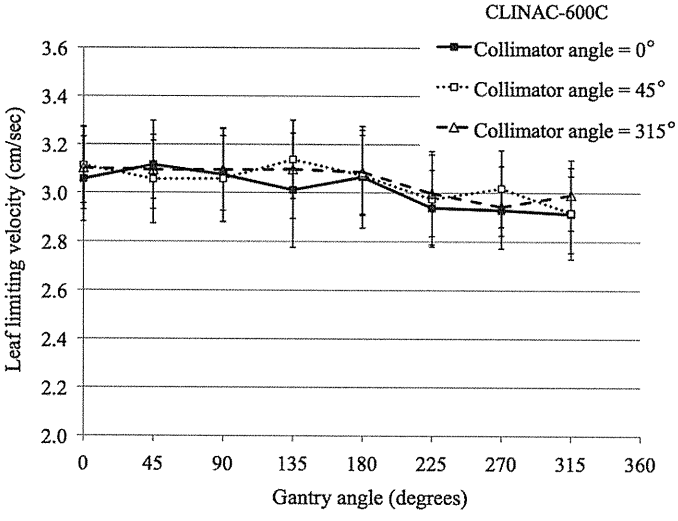

Figure 5. The mean leaf LVs at each gantry angle with three collimator angles of 0°, 45° and 315° for CLINAC-600C. Error bars shown correspond to one standard deviation.

Figure 8 shows the percentage of beam hold time of the elapsed time at 0° of collimator angle. The percentages and bars show mean values and standard deviation (SD) of 15 measurements. The percentage of beam hold time was maximum at a gantry angle of 270° for all three conditions. In CLINAC-21EX, the percentage of beam hold time was approximately half that when only central 5 mm leaves moved compared to that when all leaves moved.

Figure 9 shows the leaf position and gap width inconsistencies for various leaf velocities of 1.5 cm s^{-1} and 2.5 cm s^{-1} with a collimator angle of 0° for CLINAC-21EX. These measured data in figure 9 show an example of 15 measurements, and show the mean values of twenty

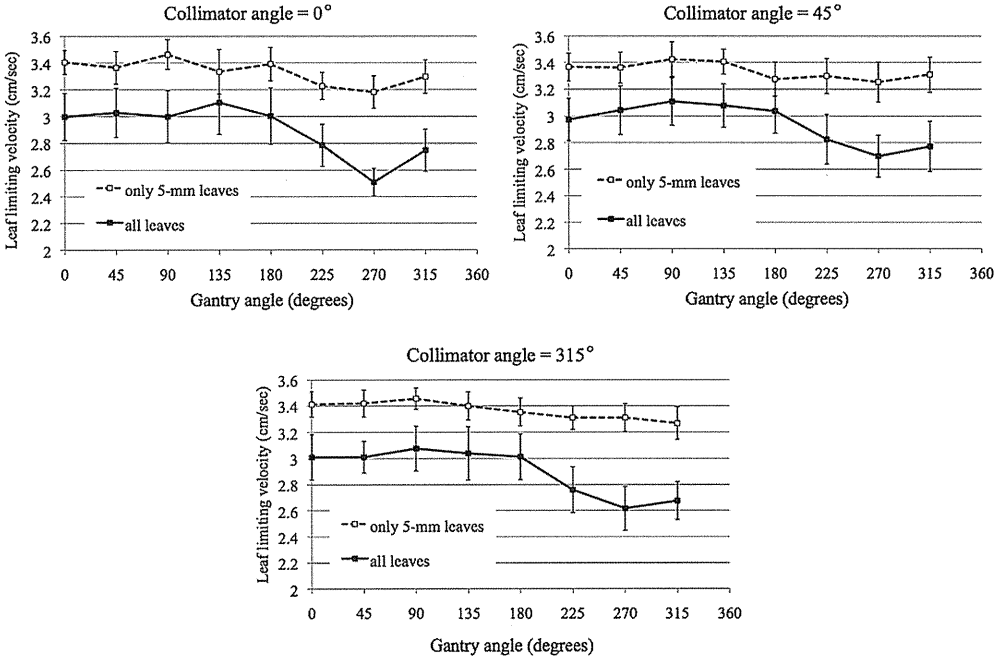

Figure 6. Results of LVs for CLINAC-21EX when all 60 pairs of leaves or only 40 central pairs of 5 mm leaves moved. Error bars shown correspond to one standard deviation.

Table 1. Summary of limiting velocity of leaves in three collimator angles for the two accelerators.

Collimator angle		0°		45°		315°	
		Ave. ± SD (cm s^{-1})	Range (cm s^{-1})	Ave. ± SD (cm s^{-1})	Range (cm s^{-1})	Ave. ± SD (cm s^{-1})	Range (cm s^{-1})
CLINAC-21EX	All leaves	2.90 ± 0.20	2.51–3.10	2.94 ± 0.16	2.70–3.11	2.90 ± 0.18	2.62–3.08
	5 mm leaves	3.33 ± 0.09	3.18–3.46	3.34 ± 0.06	3.25–3.43	3.37 ± 0.07	3.27–3.46
CLINAC-600C		3.01 ± 0.08	2.91–3.12	3.04 ± 0.07	2.92–3.14	3.05 ± 0.06	2.94–3.10

1 cm leaves and forty 5 mm leaves. The horizontal axis shows gantry angles, while the vertical axis shows the difference between the expected and actual leaf positions. The difference in the gap width was calculated by subtracting the gap width of the actual position from that of the expected position. Asterisks (*) indicate results when only 5 mm leaves were moved. As mentioned above, due to the delay time of 50 ms, the actual position is always delayed against the expected position for both leading and trailing leaves. While relative leaf position inconsistencies were within 1 mm at leaf velocities from 0.5 to 2.0 cm s^{-1}, they were more than 1 mm when the leaf velocity exceeded 2.0 cm s^{-1}. In addition, the deviations in the leaf relative position inconsistencies tended to increase as they traveled against gravity, in this case at gantry angles around 270°. At 90°, the leaves also experience gravitational effects, but since the leaves are traveling with the gravitational force, the position differences are not as pronounced. The inconsistencies in the gap width were negated by position inconsistencies

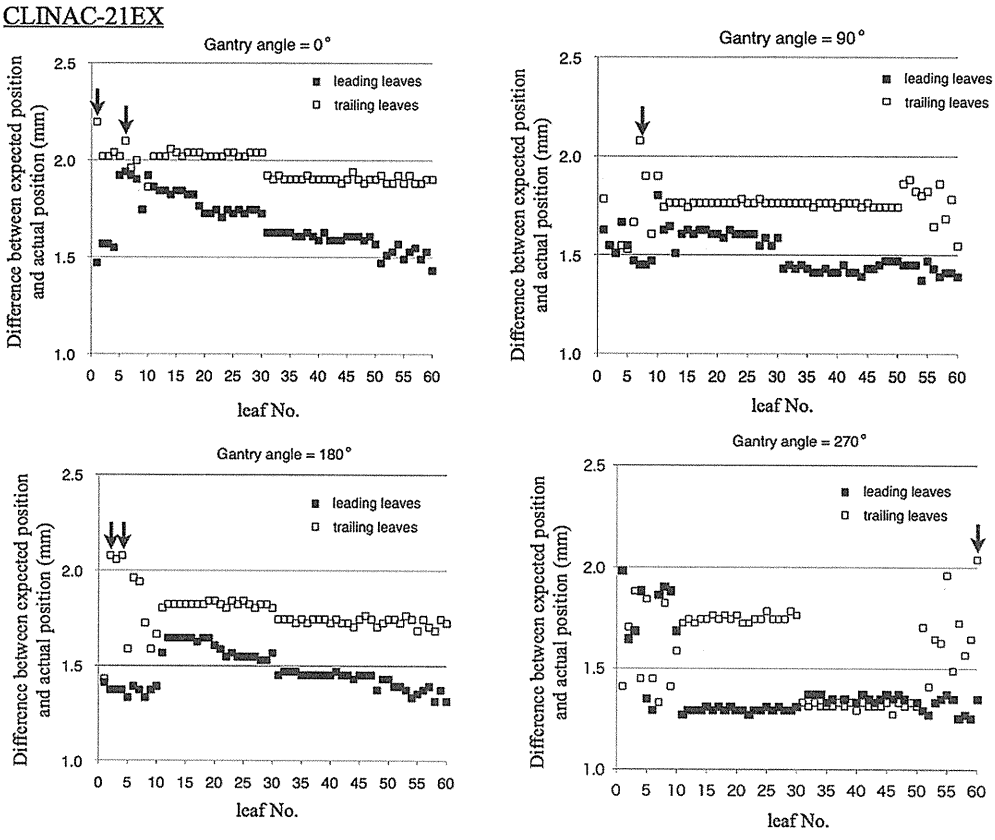

Figure 7. The differences in the MLC position between expected and actual positions for each leaf pair for CLINAC-21EX when the beam hold occurred.

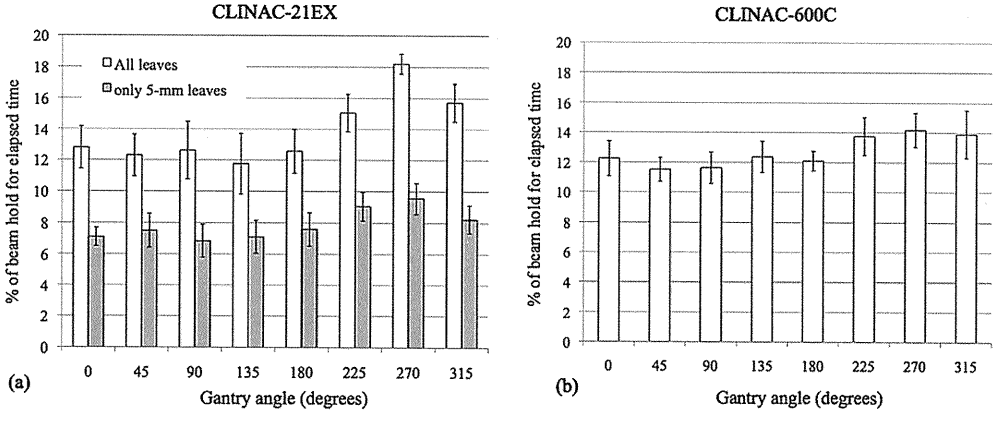

Figure 8. The percentage of beam hold time of the elapsed time at 0° of collimator angle. (a) CLINAC-21EX, (b) CLINAC-600C.

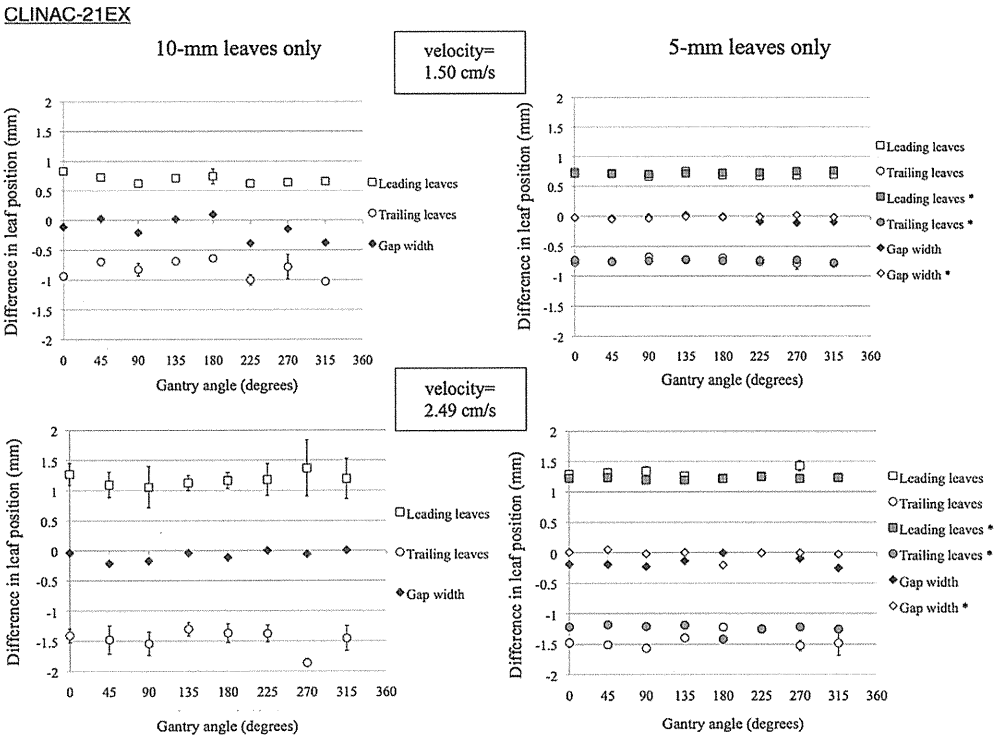

Figure 9. The leaf position and gap width inconsistencies for various leaf velocities of 1.5 cm s^{-1} and 2.5 cm s^{-1} with a collimator angle of 0° of CLINAC-21EX.

of the leading and trailing leaves. Therefore, the gap width showed acceptable values. Also, the CLINAC-600C accelerators showed a similar tendency. The maximum inconsistency in the gap width of −0.39 mm was recorded for 1 cm leaves of CLINAC21EX with a velocity of 1.5 cm s^{-1} and a gantry angle of 225°.

4. Discussion

Many publications have documented the evaluation of DMLC quality assurance (LoSasso *et al* 1998, 2001, Chui *et al* 1996, Ling *et al* 2008). In the present study, we created a DMLC file in which the MLC velocity was constantly accelerated, and the dynamic irradiation was delivered at various collimator and gantry angles. We used of a log file to evaluate leaf LV and leaf position at various collimator and gantry angles.

Litzenberg *et al* described 'effective limiting velocity' using the DMLC tolerance, the delay time and α (a factor to account for the variation in the delay) (Litzenberg *et al* 2002a). As noted by their report, the effective limiting velocity (ELV) of the MLC was shown by ELV = $x_{\mathrm{tol}}/(\alpha\, t_{\mathrm{delay}})$, where x_{tol} is DMLC tolerance, t_{delay} is the delay time between accelerator control and LMC and α is a factor to account for the variation in the delay. According to Litzenberg *et al*, the ELV is defined as the maximum leaf velocity within the leaf position tolerance, and α has been determined to be 1.4. Although the leaf LV in this study was defined when beam hold occurred, we tried to estimate α with the same equation for the measured LVs. Figure 10 shows the calculated α of each gantry angle and collimator angle = 0° of CLINAC-

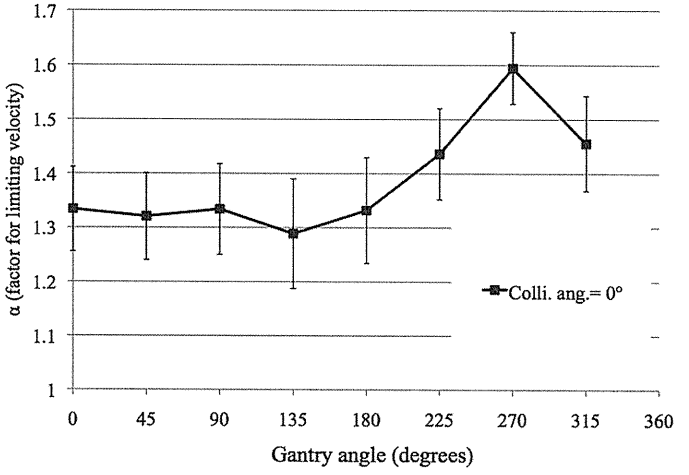

Figure 10. The calculated α of each gantry angle and collimator angle = 0° of CLINAC-21EX when all leaves moved.

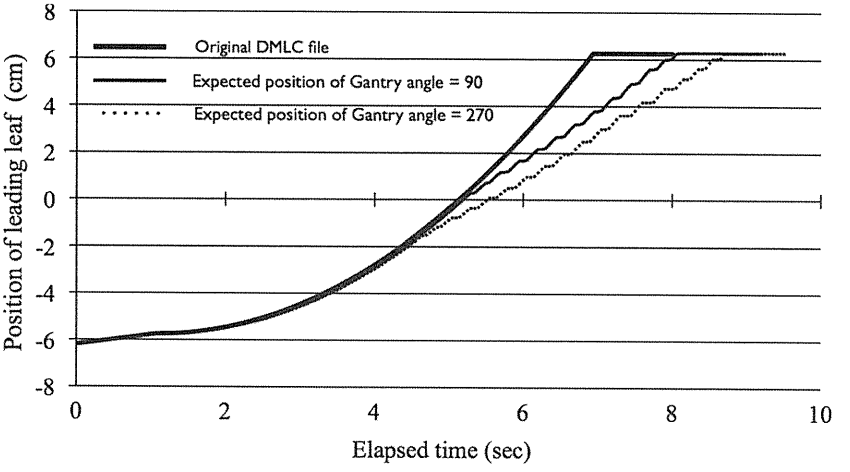

Figure 11. An example of the original DMLC file, and the expected leaf positions at 90° and 270°gantry angles with a collimator angle of 0° for CLINAC-21EX when all 60 pairs of leaves moved.

21EX when all leaves were moved. Fifteen measurements were performed for each gantry angle. The mean value and SD of α at a gantry angle = 0° for the DMLC tolerance of 2 mm was 1.34 ± 0.08. The α values ranged from 1.29 to 1.59. These values almost agreed with the α of Litzenberg *et al.* Therefore, these values should be measured and applied appropriately to each accelerator.

The minimum LV of CLINAC-21EX and CLINAC-600C were observed at a gantry angle of 270° or 315° with a collimator angle of 0°, which corresponds to a situation where the leaves are traveling opposite to the gravitational force. The LMC recorded signals from primary feedback every 50 ms during the dynamic irradiation and calculated the expected leaf position after 50 ms. Figure 11 shows an example of the original DMLC file, and the expected leaf positions at 90° and 270° gantry angles with a collimator angle of 0° for CLINAC-21EX

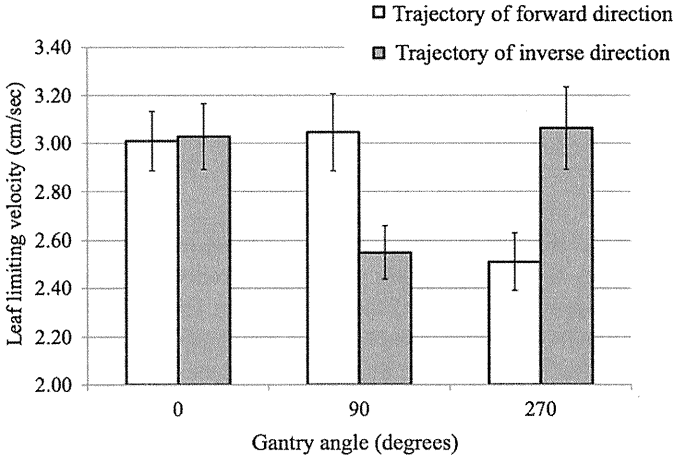

Figure 12. Comparison of leaf limiting velocities between trajectory in the forward direction and inverse direction at gantry angles of 0°, 90° and 270° when all leaves of CLINAC-21EX moved.

when all 60 pairs of leaves moved. The difference between the original DMLC file and the expected position of each leaf reveals the dependence of LV on the gantry and collimator angles. Before getting these position data, calibration of MLCs was carried out. The result of the 1 mm wide picket fence pattern (Chui *et al* 1996) and the stability of MLC output (LoSasso *et al* 2001) at gantry angles of 0°, 90°, 180° and 270° were taken as tolerance levels. As for gantry angles of 0°, 90° and 270° of CLINAC-21EX, we measured the leaf LV of trajectory in the forward direction and the trajectory in the inverse direction for 15 measurements when all leaves of CLINAC-21EX were moved. As a result, the leaf LV between gantry angles of 90° and 270° reversed (as shown in figure 12). Therefore, it seems that the expected position of the leaves was modified at all times for the difference in the influence of gravity and the load to the control motor of the MLC. The cause of the reduction in the LV for CLINAC-21EX was a delay in the motion of 1 cm leaves (as shown in figure 6). Therefore, when the planning of IMRT includes a large field or an off-axis field using 1 cm leaves, it is necessary to pay attention to the setting of the maximum leaf velocity and the dose rate related to the velocity, as well as to the relationship of the MU and DMLC segments in the TPS.

The actual position is always delayed against the expected position for both leading and trailing leaves, and the position differences of leading leaves and trailing leaves with respect to the plan increased with the acceleration of the leaf velocity. However, the differences in the gap width were negated by position errors of leading and trailing leaves (figure 9). The expected and actual leaf positions at same time of the log files disagreed due to the delay time between the accelerator controller and LMC. The monitor of dynamic leaf tolerance controls the leaves using the difference in the expected and actual positions at same time. Therefore, it is difficult to present the absolute positioning error of the leaves. In this study, the leaf position error of log files was estimated with relative inconsistency between the expected and actual leaf positions, but from results of figure 9, a relative inconsistency between the expected and actual leaf position can be shown by leaf velocity (cm s^{-1}) $\times$ delay time (s). For evaluation of the DMLC performance, the measurements changed with the influence of gravity, and therefore the mechanical loads of the leaves at various gantry and collimator angles must be considered, and this measurement method can be utilized for routine DMLC quality assurance and reproduced easily.

When the leaf position errors between the expected and actual positions are beyond the dynamic leaf position tolerance, beam hold occurs. When beam hold occurs frequently, the accuracy of the delivered dose becomes inferior and the treatment time increases (Litzenberg *et al* 2002a, LoSasso *et al* 1998). Therefore, the setting of treatment parameters without beam holds is necessary. The cause for the gantry angle and collimator angle dependence of the LV is the variation in the gravitational force relative to the leaf travel direction. Therefore, the verification for dose distributions on a per-field basis should be measured at the same gantry and collimator angles as they are planned. If unacceptable leaf position errors are observed, MLC maintenance may be warranted, for example to relieve stickiness of the leaves. In general, the performance will be better if the leaves in the sliding pattern are not required to move against gravity, so it is recommended to reverse the travel direction in the treatment plan, delivering the same fluence pattern, such that it is in the same direction as gravity.

Acknowledgments

The authors are grateful to Michelle Svatos, PhD (Translational Research Oncology Systems, Varian Medical Systems), and Katsutaro Kaneko (Varian Medical Systems, Japan) for their constructive comments on the preparation of this paper. Finally, the authors want to thank all personnel of the Radiation Treatment Therapy Department of Kinki University Hospital, who helped during this study.

References

Buonamici F B, Compagnucci A, Marrazzo L, Russo S and Bucciolini M 2007 An intercomparison between film dosimetry and diode matrix for IMRT quality assurance *Med. Phys.* **34** 1372–9

Chao K S, Deasy J O, Markman J, Haynie J, Perez C A, Purdy J A and Low D A 2001 A prospective study of salivary function sparing in patients with head-and-neck cancers receiving intensity-modulated or three-dimensional radiation therapy: initial results *Int. J. Radiat. Oncol. Biol. Phys.* **49** 907–16

Chui C S, Spirou S and LoSasso T 1996 Testing of dynamic multileaf collimation *Med. Phys.* **23** 635–41

Ezzell G A, Galvin J M, Low D, Palta J R, Rosen I, Sharpe M B, Xia P, Xiao Y, Xing L and Yu C X 2003 Guidance document on delivery, treatment planning, and clinical implementation of IMRT: report of the IMRT Subcommittee of the AAPM Radiation Therapy Committee *Med. Phys.* **30** 2089–115

Greer P B and Popescu C C 2003 Dosimetric properties of an amorphous silicon electronic portal imaging device for verification of dynamic intensity modulated radiation therapy *Med. Phys.* **30** 1618–27

Jursinic P A and Nelms B E 2003 A 2D diode array and analysis software for verification of intensity modulated radiation therapy delivery *Med. Phys.* **30** 870–9

Lee N, Xia P, Quivey J M, Sultanem K, Poon I, Akazawa C, Akazawa P, Weinberg V and Fu K K 2002 Intensity-modulated radiotherapy in the treatment of nasopharyngeal carcinoma: an update of the UCSF experience *Int. J. Radiat. Oncol. Biol. Phys.* **53** 12–22

Li J G, Dempsey J F, Ding L, Liu C and Palta J R 2003 Validation of dynamic MLC-controller log files using a two-dimensional diode array *Med. Phys.* **30** 799–805

Ling C C, Zhang P, Archambault Y, Bocanek J, Tang G and Losasso T 2008 Commissioning and quality assurance of RapidArc radiotherapy delivery system *Int. J. Radiat. Oncol. Biol. Phys.* **72** 575–81

Litzenberg D W, Moran J M and Fraass B A 2002a Incorporation of realistic delivery limitations into dynamic MLC treatment delivery *Med. Phys.* **29** 810–20

Litzenberg D W, Moran J M and Fraass B A 2002b Verification of dynamic and segmental IMRT delivery by dynamic log file analysis *J. Appl. Clin. Med. Phys.* **3** 63–72

LoSasso T, Chui C S and Ling C C 1998 Physical and dosimetric aspects of a multileaf collimation system used in the dynamic mode for implementing intensity modulated radiotherapy *Med. Phys.* **25** 1919–27

LoSasso T, Chui C S and Ling C C 2001 Comprehensive quality assurance for the delivery of intensity modulated radiotherapy with a multileaf collimator used in the dynamic mode *Med. Phys.* **28** 2209–19

Mell L K, Mehrotra A K and Mundt A J 2005 Intensity-modulated radiation therapy use in the US, 2004 *Cancer* **104** 1296–303

Mundt A J, Lujan A E, Rotmensch J, Waggoner S E, Yamada S D, Fleming G and Roeske J C 2002 Intensity-modulated whole pelvic radiotherapy in women with gynecologic malignancies *Int. J. Radiat. Oncol. Biol. Phys.* **52** 1330–7

Otto K 2008 Volumetric modulated arc therapy: IMRT in a single gantry arc *Med. Phys.* **35** 310–7

Palta J, Kim S, Li J and Liu C 2003 Tolerance limits and action levels for planning and delivery of IMRT *Med. Phys.* **30** 1395

Stell A M, Li J G, Zeidan O A and Dempsey J F 2004 An extensive log-file analysis of step-and-shoot intensity modulated radiation therapy segment delivery errors *Med. Phys.* **31** 1593–602

Wijesooriya K, Bartee C, Siebers J V, Vedam S S and Keall P J 2005 Determination of maximum leaf velocity and acceleration of a dynamic multileaf collimator: implications for 4D radiotherapy *Med. Phys.* **32** 932–41

Yu C X 1995 Intensity-modulated arc therapy with dynamic multileaf collimation: an alternative to tomotherapy *Phys. Med. Biol.* **40** 1435–49

Zeidan O A, Li J G, Ranade M, Stell A M and Dempsey J F 2004 Verification of step-and-shoot IMRT delivery using a fast video-based electronic portal imaging device *Med. Phys.* **31** 463–76

Zelefsky M J, Fuks Z, Hunt M, Yamada Y, Marion C, Ling C C, Amols H, Venkatraman E S and Leibel S A 2002 High-dose intensity modulated radiation therapy for prostate cancer: early toxicity and biochemical outcome in 772 patients *Int. J. Radiat. Oncol. Biol. Phys.* **53** 1111–6

Zhu X R, Jursinic P A, Grimm D F, Lopez F, Rownd J J and Gillin M T 2002 Evaluation of Kodak EDR2 film for dose verification of intensity modulated radiation therapy delivered by a static multileaf collimator *Med. Phys.* **29** 1687–92

Zygmanski P, Kung J H, Jiang S B and Chin L 2003 Dependence of fluence errors in dynamic IMRT on leaf-positional errors varying with time and leaf number *Med. Phys.* **30** 2736–49

ELSEVIER

Int. J. Radiation Oncology Biol. Phys., Vol. 77, No. 2, pp. 350–356, 2010

0360-3016/$–see front matter

doi:10.1016/j.ijrobp.2009.05.025

CLINICAL INVESTIGATION **Lung**

RADIATION TREATMENT PLANNING USING POSITRON EMISSION AND COMPUTED TOMOGRAPHY FOR LUNG AND PHARYNGEAL CANCERS: A MULTIPLE-THRESHOLD METHOD FOR [^{18}F]FLUORO-2-DEOXYGLUCOSE ACTIVITY

MITSURU OKUBO, M.D.,* YASUMASA NISHIMURA, M.D., PH.D.,* KIYOSHI NAKAMATSU, M.D., PH.D.,* MASAHIKO OKUMURA, R.T.,† TORU SHIBATA, M.D., PH.D.,* SHUICHI KANAMORI, M.D., PH.D.,* KOUHEI HANAOKA, R.T.,† AND MAKOTO HOSONO, M.D., PH.D.‡

Departments of *Radiation Oncology, †Central Radiological Service, and ‡PET, Kinki University School of Medicine, 377-2 Ohno-Higashi, Osaka-Sayama, Osaka 589-8511, Japan

Purpose: Clinical applicability of a multiple-threshold method for [^{18}F]fluoro-2-deoxyglucose (FDG) activity in radiation treatment planning was evaluated.

Methods and Materials: A total of 32 patients who underwent positron emission and computed tomography (PET/CT) simulation were included; 18 patients had lung cancer, and 14 patients had pharyngeal cancer. For tumors of ≤2 cm, 2 to 5 cm, and >5 cm, thresholds were defined as 2.5 standardized uptake value (SUV), 35%, and 20% of the maximum FDG activity, respectively. The cervical and mediastinal lymph nodes with the shortest axial diameter of ≥10 mm were considered to be metastatic on CT (LNCT). The retropharyngeal lymph nodes with the shortest axial diameter of ≥5 mm on CT and MRI were also defined as metastatic. Lymph nodes showing maximum FDG activity greater than the adopted thresholds for radiation therapy planning were designated LNPET-RTP, and lymph nodes with a maximum FDG activity of ≥2.5 SUV were regarded as malignant and were designated LNPET-2.5 SUV.

Results: The sizes of gross tumor volumes on PET (GTVPET) with the adopted thresholds in the axial plane were visually well fitted to those of GTV on CT (GTVCT). However, the volumes of GTVPET were larger than those of GTVCT, with significant differences ($p < 0.0001$) for lung cancer, due to respiratory motion. For lung cancer, the numbers of LNCT, LNPET-RTP, and LNPET-2.5 SUV were 29, 28, and 34, respectively. For pharyngeal cancer, the numbers of LNCT, LNPET-RTP, and LNPET-2.5 SUV were 14, 9, and 15, respectively.

Conclusions: Our multiple thresholds were applicable for delineating the primary target on PET/CT simulation. However, these thresholds were inaccurate for depicting malignant lymph nodes. © **2010 Elsevier Inc.**

FDG, Threshold value, Radiation treatment planning, Positron emission tomography.

INTRODUCTION

Positron emission and computed tomography (PET/CT) fusion is used for the purpose of radiation treatment planning (RTP) in patients with non-small-cell lung cancer (NSCLC), esophageal carcinoma, head and neck cancer, rectal cancer, etc. (1–12). The benefits of using PET/CT for RTP are obvious. In the delineation of the gross tumor volume (GTV), [^{18}F]fluoro-2-deoxyglucose (FDG)-PET/CT images can significantly reduce interobserver variation (13). Faria *et al.* (1) and Erdi *et al.* (14) reported that RTP based on CT and PET fusion images was useful for delineating tumors from atelectasis in patients with NSCLC.

Because the size of the GTV derived from FDG accumulation changes significantly depending on the threshold value, the threshold value can affect the clinical target delineation. Erdi *et al.* reported that 36% to 44% of the maximum FDG activity was appropriate for delineating target volumes larger than 4 cm^3, in a static phantom study (15).Recently, thresholds calculated by more complex algorithms containing the mean activity of spheres and background activity were proposed (Table 1) (16–18). However, an appropriate threshold value for the target delineation has not been defined.

The planning target volume (PTV) contains margins for internal motion and setup error. For lung tumors, respiratory

Reprint requests to: Yasumasa Nishimura, M.D., Department of Radiation Oncology, Kinki University School of Medicine, 377-2 Ohno-Higashi, Osaka-Sayama, Osaka 589-8511, Japan. Tel: (+81) 72-366-0221; Fax: (+81) 72-368-2388; E-mail: ynishi@med.kindai.ac.jp

This study was supported in part by a Grant-in-Aid for Scientific Research (17591300) from the Ministry of Education, Science, Sports, and Culture, Japan, and by a Grant-in-Aid in 2006 from the Association for Nuclear Technology in Medicine.

This paper was presented at the 5th Annual Japan-US Cancer Therapy Symposium and the 5th Annual S. Takahashi Memorial International Joint Symposium, Sendai, Miyagi, Japan, September 7-9th, 2007.

Conflict of interest: none.

Received Sept 30, 2008, and in revised form Feb 13, 2009. Accepted for publication May 12, 2009.

Table 1. Literature review of thresholds for contouring phantoms or GTVs with PET

Study (ref.)	No. of patients or phantom	Threshold
Erdi *et al.* (15)	Static phantom	42%*
Nestle *et al.* (16)	25 (NSCLC)	$(0.15 \times I_{mean}) + I_{background}$
Black *et al.* (17)	Static phantom	0.307 × (mean target SUV) + 0.588
Davis *et al.* (18)	Static phantom	Bgd + 0.41 × (Sig_{max} – Bgd)
Ford *et al.* (20)	Static phantom 8 (head and neck cancer)	42%*
Deniaud-Alexandre *et al.* (21)	101 (NSCLC)	50%*
Caldwell *et al.* (22)	Moving phantom	15%*
Nagel *et al.* (23)	Moving phantom	34%*
Hong *et al.* (24)	19 (NSCLC)	2.5 SUV
Biehl *et al.* (25)	20 (NSCLC)	<3 cm: 42%* 3-5 cm: 24%* >5 cm: 15%*
Yaremko *et al.* (26)	Static and moving phantom	Static: 50%* Moving: 25%* Gated breath hold
Ashamalla *et al.* (27)	19 (NSCLC)	Visual interpretation

* Percentage of maximal FDG activity.

motion is the major contributor to internal motion. Presently, CT simulation is the standard for RTP. However, conventional CT images cannot reflect internal motion because CT provides only snapshot images of a moving tumor. On the other hand, it takes a few minutes to acquire PET images. Thus, PET images are influenced by internal motion and have the potential to delineate an internal target volume (ITV) (19, 22).

Previously, we performed static and moving phantom experiments and determined an appropriate threshold value for target delineation in PET images at our institution (19). Appropriate threshold values for target delineation ranged from 30% to 40% of the maximum FDG activity for spheres of 22 to 37 mm. Table 1 summarizes the various thresholds for target delineation with PET proposed by various investigators. In several studies, the target was delineated by PET using a simple threshold: a percentage of the maximum FDG activity (15, 20–24). However, several investigators have reported that the use of a single-threshold model for delineating the GTV with PET/CT is not sufficient because of the effects of target size, motion, and image reconstruction parameters (25, 26). Thus, we adopted multiple thresholds for target delineation with PET, dependent on the target size, according to our phantom studies (19) and published our findings (25). The purpose of this study was to evaluate the clinical applicability of our multiple-thresholds method in RTP, using PET/CT for lung and pharyngeal cancers.

METHODS AND MATERIALS

Study population

This study population consisted of 32 patients who underwent PET/CT simulation between January 2006 and September 2007. Eighteen patients had lung cancers, and 14 patients had pharyngeal cancers. Performance status for most patients was 0 or 1. No distant metastatic lesions were detected by pretreatment examination including physical examinations and CT scans of the chest and upper abdomen. Bone scintigraphy and brain CT or MRI were not routinely performed. Patient characteristics are shown in Table 2. Informed written consent for PET/CT simulation was obtained from all patients.

Table 2. Patient and tumor characteristics

Patient or tumor	No. of patients with pharynx tumors	No. of patients with lung tumors
Total no. of patients	14	18
Age (y)		
Median	56	69
Range	19-79	44-83
Gender		
Male	11	16
Female	3	2
Performance status		
0	12	11
1	2	4
2	0	3
Stage before PET/CT simulation*		
I	4	2
II	1	2
III	4	14
IV	5	0
Histology		
	Sqcc: 13 Lymphoepithelioma: 1	Sqcc: 8 Adenocarcinoma: 6 Scc: 2 Carcinoma: 2
Primary site		
	Nasopharynx: 10 Oropharynx: 3 Hypopharynx: 1	Upper lobe: 8 Middle lobe: 8 Lower lobe: 2

Abbreviations: Sqcc = squamous cell carcinoma; Scc = small-cell carcinoma.

* According to the 2002 International Union Against Cancer classification.

PET/CT simulation protocol

Patients were injected with 3 MBq/kg FDG and were left in the designated "quiet room" for an uptake period of 60 min. After this time period, patients were placed on a specialized flat table for RTP. For reproducibility, one anterior and two lateral reference points were marked on the patient, using laser marks. Patients with pharyngeal cancer were positioned in the supine position with a thermoplastic mask (S-type; MED-TEC, Orange City, IA). Patients with lung cancer were positioned in the supine position without immobilization. Both PET and CT scans of the region of interest were obtained. The patients were asked to breathe normally during PET/CT scan acquisition, and no specific breathing instructions were given. After the region of interest was scanned, a full-body PET/CT scan was performed for staging purposes. About 45 min was required to complete the full-body PET/CT scan. PET/CT images were reviewed by an experienced nuclear medicine physician/radiologist and a radiation oncologist.

PET/CT acquisition

Each patient was scanned with an integrated PET (Biograph)/CT (Somatom Emotion Duo) unit (Siemens Medical Solutions, Hoffmann Estates, IL). CT scans were acquired in the spiral mode, with a slice thickness of 2 mm, a pitch of 6 mm, at 130 kV and 55 mA. The translation speed of the couch is 7.4 mm/sec. All CT images were acquired using a matrix of 512 × 512 pixels.Voxel dimensions were 0.9 mm × 0.9 mm × 2.0 mm. Eighteen patients (56%) were given 100 ml of intravenous contrast (300 mg/ml iodine) for the CT component of the PET/CT studies.

The examination was started at 45 to 60 min after injection of 3 MBq/kg FDG in the three-dimensional mode, using an axial field of view of 404 mm (three bed positions). The time for one-bed position (162 mm) scan was 100 sec. All PET images were acquired using a matrix of 128 × 128 pixels. At a distance of 10 cm from the center of the field of view, the full width at half maximum reached 7.4 mm × 7.4 mm × 7.1 mm in the x, y, and z directions, respectively. A Fourier rebinning algorithm was combined with an ordered subsets expectation-maximization reconstruction (eight subsets, two iterations). Voxel dimensions were 4.5 mm × 4.5 mm × 2.0 mm.

Target volume delineation

After PET/CT scans were performed, the PET and CT data sets were converted to digital imaging and communication in medicine (DICOM) format and transferred to a radiation treatment system (Eclipse instrument; Varian Medical Systems, Palo Alto, CA). To compare the CT-based target volume with the PET-based target volume, GTVs of primary lesions were contoured by one observer without knowledge of other modality images. First, the GTV of primary lesions on CT (GTVCT) was contoured using only CT for lung cancer and both CT and MRI for pharyngeal cancer. No fusion images of CT and MRI were available. The window width and level for GTVCT delineation of lung cancer were 1,500 Hounsfield units (HU) and −550 HU as lung window settings, respectively, and those of pharyngeal cancer were 300 HU and 50 HU, respectively, as soft tissue window settings.

For contouring GTVs of primary lesions on PET (GTVPET), three threshold levels were adopted in this study. In our previous phantom experiments, 35% of the maximum FDG activity was appropriate for GTV delineation of spheres from 2.2 to 3.7 cm with PET (19). However, this threshold was inappropriate for tumors of ≤2 cm and those >5 cm, clinically. Because tumor size and motion affect SUV measurement (19, 25, 26), a single-threshold method is inadequate for GTV delineation on PET. Thus, for tumors of ≤2 cm, a threshold value of 2.5 SUV was adopted. For tumors of 2 to 5 cm and those >5 cm, threshold values of 35% and 20% of the maximum FDG activity of the primary tumors were adopted, respectively. These thresholds were determined according to our phantom study (19) and published study (25).

The volumes of primary tumors and the maximum diameters in the axial plane were compared between GTVCT and GTVPET. Primary tumors that could not be depicted clearly by CT were excluded from the analysis of volume comparison.

Definitions of malignant lymph nodes

For lung cancer, mediastinal lymph nodes with the shortest axial diameter of ≥10 mm were considered to be malignant based on CT (LNCT) (28). For pharyngeal cancer, cervical lymph nodes with the shortest axial diameter of ≥10 mm and retropharyngeal lymph nodes with the shortest axial diameter of ≥5 mm on CT or MRI were defined as malignant (LNCT/MRI). Lymph nodes of borderline size with abnormal enhancement were also indications of malignancy (29, 30).

Lymph nodes with maximum FDG activity of ≥2.5 SUV were regarded as malignant and defined as LNPET-2.5 SUV (31–33). Lymph nodes with maximum FDG activity larger than the adopted threshold value for RTP were defined as LNPET-RTP.

RESULTS

Of the 32 patients included, distant metastases were found in 2 patients, using PET/CT simulation. For the 2 patients, the treatment intent was altered from definitive to palliative. These 2 patients were also included in this analysis. For lung cancer patients, 4 of 18 patients could not receive the planned prescription dose because of pneumonia or the patient's wishes. The 2-year survival rate for the remaining 14 patients with stages I to III was 56%. All 14 patients with pharyngeal cancer received the planned prescription dose. The 2-year survival rate for the 14 patients was 93%.

Size and volume of GTV

The mean maximum ± standard deviation (SD) FDG activity of the 32 primary tumors was 4.4 ± 1.6 SUV (range, 3.3–22.2 SUV). The mean maximum ± SD FDG activities of primary tumors of ≤2 cm, 2 to 5 cm, and >5 cm were 4.0 ± 1.0 SUV (range, 3.3–4.7 SUV), 9.3 ± 3.8 SUV (4.6–16.6 SUV), and 15.8 ± 4.3 SUV (8.2–22.2 SUV), respectively. The maximum FDG activities of tumors >5 cm were significantly larger than that of tumors 2 to 5 cm (unpaired t test, $p = 0.0008$).

Delineation of GTV was unclear on PET and/or CT for 2 of the 18 primary lung tumors due to interstitial pneumonia or tumor necrosis. The volumes of the remaining 16 primary lung tumors were evaluated. The mean maximum ± SD diameter of tumors in the axial plane on CT was 4.9 ± 1.7 cm (range, 2.6–7.5 cm). The maximum diameters of 10 tumors ranged from 2 to 5 cm and those of 6 tumors were >5 cm. No tumors were ≤2 cm in diameter. The maximum ± SD diameter of GTVPET in the axial plane on the level of the largest GTVCT was 5.2 ± 1.7 cm (range, 2.6–9.4 cm). There were no significant differences in maximum diameter between GTVPET and GTVCT(paired-t test, $p = 0.845$).